ECE 445

SENIOR DESIGN LABORATORY

FINAL REPORT

HARMONEX

Team #8

ALAN LU (jialin8@illinois.edu)
RUBIN DU (rd25@illinois.edu)

TA: Bill Yang

December 10, 2025

Abstract

This report presents HARMONEX, a lightweight, modular upper-limb exoskeleton designed to assist users in lifting and carrying heavy objects while preserving natural movement when assistance is not required. The system addresses the limitations of existing exoskeletons—namely bulk, weight, and lack of backdrivability—by employing a dual-actuator architecture with selectively engageable dog clutches. At the elbow joint, a brushless DC (BLDC) motor drives a three-stage planetary gearbox (64:1 reduction) for dynamic lifting, while a high-torque servo actuates a spur-bevel-rack linkage train for steady holds and precise positioning. Both drive trains default to a disengaged state, allowing free joint motion with minimal reflected inertia when idle.

A TI C2000 microcontroller coordinates actuation based on electromyography (EMG) signals and joint-angle feedback. A compact multilayer perceptron (12–24–16–3 architecture, 787 parameters) predicts user intent with approximately 7° mean absolute error and classifies workload state with over 90% accuracy, enabling responsive torque assistance within 150 ms of detected muscle activation. The power subsystem distributes energy from a 6S lithium-polymer battery through regulated 23 V, 16 V, 5 V, and 3.3 V rails, with hardware E-stop, fuse protection, and low-noise analog supplies for the EMG front-end.

Verification testing confirmed that the exoskeleton delivers $\geq$40 N·m of joint torque, supports a 10 kg payload at 0.4 m from the elbow through a full 0°–90° range of motion, and maintains stable power rails under load transients. Safety features include mechanical end-stops, thermal monitoring, clutch interlocks, and fail-safe defaults that return the system to a passive, backdrivable state upon fault detection. The resulting design demonstrates a practical approach to wearable assistive robotics that balances torque capacity, user comfort, and operational safety.

Contents

1 Introduction

1.1 Problem

Lifting and carrying heavy loads is a common activity in both personal and industrial environments, yet it places significant stress on the musculoskeletal system. Repetitive loading is a leading cause of workplace injuries and long-term skeletal disorders, according to the U.S. Bureau of Labor Statistics. Existing assistive exoskeletons often remain bulky, heavy, and non-backdrivable, restricting natural movement and limiting practical daily use. A lightweight, safe, and responsive wearable device that supports users only when needed—without hindering motion when idle—remains an unmet need.

1.2 Solution

We developed **HARMONEX** (**H**ybrid-**A**ctuation **R**obotic **M**echanism for **O**mni-domain **N**eural-signal **EX**oskeleton), a lightweight, modular upper-limb assist device designed to provide powered support only when needed while remaining fully backdrivable when idle. The system integrates a BLDC planetary drive at the elbow, a high-torque servo linkage at the shoulder, dual dog clutches, custom sensing and power PCBs, and an EMG-based intent interface.

By default, both clutches are disengaged so the arm moves naturally with minimal added inertia. When lifting intent is detected, the controller engages the appropriate actuator—BLDC for dynamic high-torque motion or servo for steady holding and fine positioning. Faults automatically return the system to a safe, unpowered, backdriven state. HARMONEX thus provides meaningful assistance while remaining unobtrusive during everyday movement.

1.3 High Level Requirements

- The exoskeleton will deliver $\geq 40\ \mathrm{N \cdot m}$ of net torque at the elbow, able to lift a $10\ \mathrm{kg}$ weight located $0.40\ \mathrm{m}$ from the joint, through a $0°$–$90°$ motion at $\geq 60°/\mathrm{s}$, while the user contributes $\leq 10\%$ of the required torque.
- With a full charge, the system will operate for $\geq\ 3.0\ \mathrm{h}$ under 10 per minute of a $0°$–$90°$ lift of a $10\ \mathrm{kg}$ payload ($2\ \mathrm{s}$ lift, $2\ \mathrm{s}$ hold, $2\ \mathrm{s}$ lower), with power active during idle intervals.
- The control system will use EMG-based motion detection with $\leq 150\ \mathrm{ms}$ command latency and $\leq 5\%$ false-activation rate in normal use, and the clutch will engage or disengage in $\leq 200\ \mathrm{ms}$ while limiting peak torque ripple to $\leq 15\%$ of torque.

1.4 Block Diagram

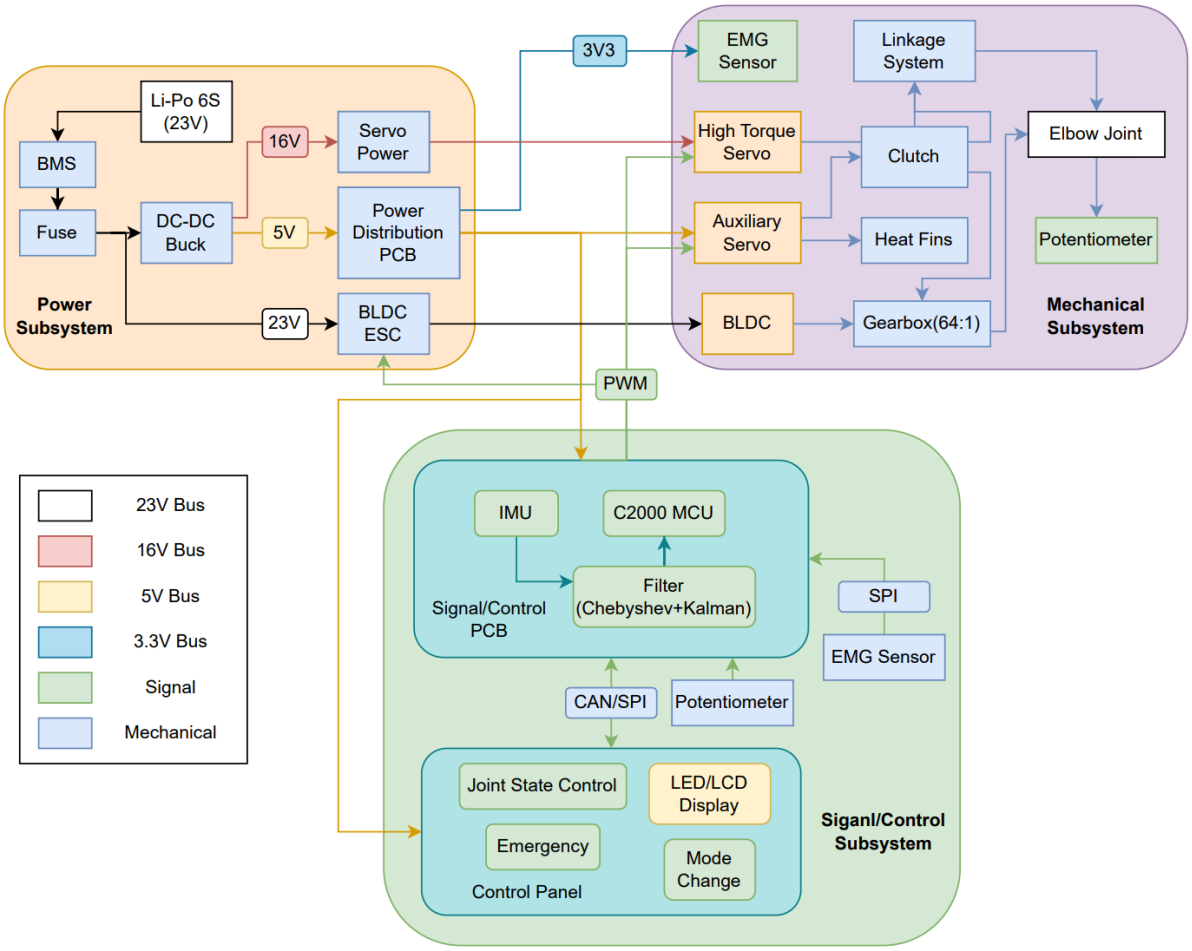

Figure 1: Block Diagram

The system is composed of three main subsystems: the Power Subsystem, Mechanical Subsystem, and Signal/Control Subsystem. The Power Subsystem is responsible for converting the 23 V supply from the Li-Po 6S battery into regulated 16 V, 5 V, and 3.3 V outputs to power different components across the system. The mechanical subsystem transforms electrical energy into mechanical motion and provides mechanical advantage through elements such as the gearbox, linkage, clutch, and servo mechanisms that drive the elbow joint. The Signal/Control Subsystem manages communication and coordination among sensors, actuators, the C2000 MCU, and the control interface, ensuring synchronized operation between motors, EMG input, and safety features like the emergency stop and control panel.

2 Design

2.1 Design Procedure

Discuss your design decisions for each block at the most general level: What alternative approaches to the design are possible, which was chosen, and why is it desirable? Introduce the major design equations or other design tools used; show the general form of the circuits and describe their functions.

While designing the subsystems of the project, we have considered several possible variants.

2.1.1 Mechanical Subsystem

For the mechanical subsystem, the most significant design decisions concern the architecture of the drive trains. For the BLDC drive, we compared three main reduction strategies: a planetary gearbox, a harmonic (strain-wave) drive, and a cycloidal reducer. Harmonic and cycloidal drives offer excellent torque density and very low backlash, but they demand tight machining tolerances, nontrivial flexure elements, and are difficult to prototype reliably with FDM 3D printing. In contrast, a planetary gearbox can be realized with simple spur gears, tolerates the dimensional error of printed parts more gracefully, and can be combined with metal pins and off-the-shelf bearings to achieve sufficient stiffness and torque capacity for the target load. For these reasons of manufacturability, cost, and robustness in a student-lab environment, the BLDC drive ultimately uses a planetary configuration. The total reduction for a planetary drive is given by:

$$i_{\mathrm{tot}} = i_1\, i_2\, i_3 = \prod_{k=1}^{3} i_k = \prod_{k=1}^{3} \left(1 + \frac{Z_{r,k}}{Z_{s,k}}\right) \tag{1}$$

where i_{tot} is the overall reduction ratio of the three–stage planetary gear train, and i_k is the reduction ratio of stage k. The variables $Z_{s,k}$ and $Z_{r,k}$ denote the number of teeth on the sun gear and ring gear of stage k, respectively. This expression assumes a classical planetary configuration with the ring gear fixed, the sun gear as the input, and the carrier as the output. The number of teeth on the planet gears does not explicitly appear in the ratio because it is constrained by the meshing condition $Z_{r,k} = Z_{s,k} + 2Z_{p,k}$.

For the high-torque servo drive train, we considered spur versus helical gear arrangements. Helical gears could provide smoother engagement and higher effective contact ratio, but they introduce axial thrust loads, are harder to print accurately, and require more complex alignment. Spur gears, on the other hand, are straightforward to model, print, and assemble, and they keep loads predominantly in the radial direction, which simplifies bearing and housing design. Therefore, spur gearing was selected for the servo transmission.

Finally, for the linkage coupler between the servo drive train and the forearm shell, we evaluated placing the coupler outside the armor shell versus nesting it inside the shell

volume. An external coupler simplifies access and inspection but increases the effective elbow bulk, creates snagging risks, and breaks the visual continuity of the exoskeleton. Integrating the coupler inside the shell, with a cover piece forming the inner elbow surface, protects the mechanism, improves user safety and aesthetics, and preserves a compact elbow contour. Consequently, the coupler is mounted internally and covered as part of the inner elbow armor.

2.1.2 Power Subsystem

The power network must distribute energy from a single 6S battery (23 V) to four types of loads: the BLDC drive, the high–torque servo, general 5 V peripherals, and low–noise analog/digital circuitry. At the highest level, the main architectural choice is whether to generate all supply rails directly from the 23 V battery in parallel, or to create one or two intermediate buses and cascade point–of–load converters from those buses.

A parallel distribution (23 V$\rightarrow$16 V and 23 V$\rightarrow$5 V independently) minimizes the number of conversion stages and therefore maximizes overall efficiency, since

$$\eta_{\text{tot}} = \prod_{k=1}^{N} \eta_k, \tag{2}$$

but requires multiple regulators rated for the full battery voltage and forces sensitive circuitry to share the noisy high–power domain. A cascaded approach (23 V$\rightarrow$16 V$\rightarrow$5 V) reduces component voltage stress and allows each stage to be optimized for its load, but compounds conversion losses and routes all peripheral power through the 16 V stage.

For the low–voltage domain, 3.3 V can either be generated directly from the battery or from the 5 V rail. Using the 5 V$\rightarrow$3.3 V stage keeps the step–down ratio moderate and allows the logic supply to be physically isolated from the high–current servo and BLDC branches. Likewise, the EMG circuitry requires clean ± 8 V analog rails; generating these from the 3.3 V digital rail via a boost–plus–invert topology decouples the analog ground from switching noise on the 23 V bus and improves measurement fidelity.

Finally, peripheral 5 V loads (aux servos, LEDs, sensors) are separated from the logic rail to prevent large transient currents from disturbing the ADC reference and EMG amplifier. The INA240 current sensor may be placed on the BLDC branch or battery input; isolating the BLDC current provides more actionable protection without loading the entire power path.

Overall, the chosen architecture uses a small number of high–power converters fed directly from the battery, with low–noise and analog rails generated downstream. This balances efficiency, noise isolation, regulator stress, and PCB complexity while meeting the diverse requirements of the actuators and sensing electronics.

2.1.3 Signal/Control Subsystem

For the signal and control subsystem the main architectural choice is the microcontroller platform. Candidate families included Espressif ESP32 devices, STMicroelectronics STM32

parts, and the TI C2000 series. ESP32 offers integrated WiFi/Bluetooth and is convenient for high–level communication, but its ADC performance, PWM resolution, and realtime determinism are not optimized for high–bandwidth current and position control of motors. STM32 devices provide good general–purpose performance and motor–control libraries, but still target a broad application space. In contrast, the C2000 family is specifically designed for motor control and power electronics; it provides tightly synchronized high–resolution PWM units, fast multi–channel ADCs with flexible SOC triggering, and low interrupt latency, all of which are crucial for stable torque and impedance control at kHz update rates. For this reason a C2000 device (F280049C) was selected as the main controller, while ESP32–class processors are reserved for future high–level communication if needed.

On the control–algorithm side there are several possible strategies. A simple approach is pure joint–state control, where the controller commands actuator torque to track a desired joint angle using conventional PID feedback. A more advanced alternative is a hybrid torque/impedance controller that combines joint state feedback with estimated load torque and EMG–based intent, so that the exoskeleton behaves compliantly and shares effort with the human user. The general form of the inner joint–space controller is

$$\tau_{\text{net}} = K_p, (q_d - q) + K_d, (\dot{q}d - \dot{q}) + Ki \int (q_d - q), \mathrm{d}t + \tau_g, \tag{3}$$

where q and $\dot{q}$ are the measured joint angle and velocity, q_d and $\dot{q}d$ are their desired values, Kp, K_d, and K_i are proportional, derivative, and integral gains, and τ_g is an optional gravity–compensation torque based on the estimated arm and payload weight. In the hybrid impedance mode this commanded torque is further shaped by current feedback and EMG–derived intent to allocate effort between the BLDC module and the servo.

Another important decision is whether to keep the controller on an off–the–shelf development board (such as a TI LaunchPad) or to integrate it onto a custom signal PCB. Development boards greatly reduce bring–up effort and are suitable for benchtop experiments, but they are bulky, offer limited connector flexibility, and make it difficult to control grounding, analog routing, and mechanical packaging for a wearable device. A custom PCB allows the C2000 MCU, the INA240 current sensor, level shifting, and connector layout to be co–designed with the power PCB and mechanical structure, which improves noise performance, reliability, and overall system integration.

2.2 Design Details

2.2.1 Mechanical Subsystem

The parametric view of the design and three basic views are given in the figures below.

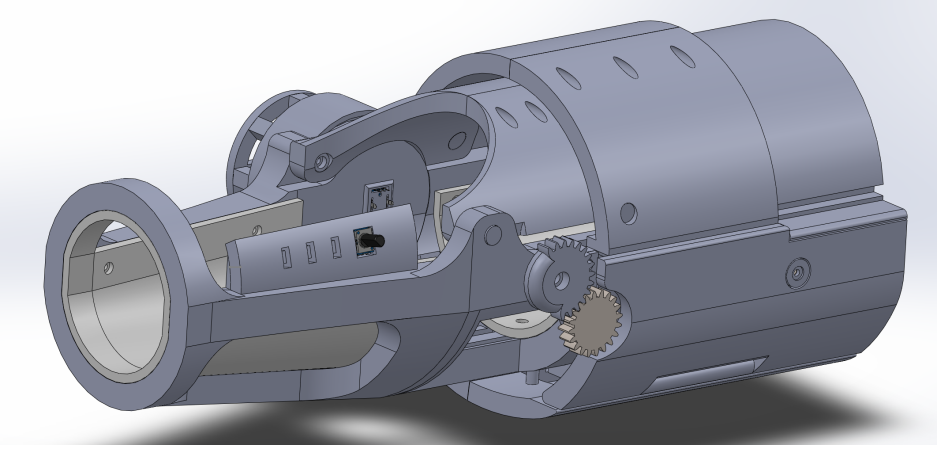

Figure 2: Parametric view

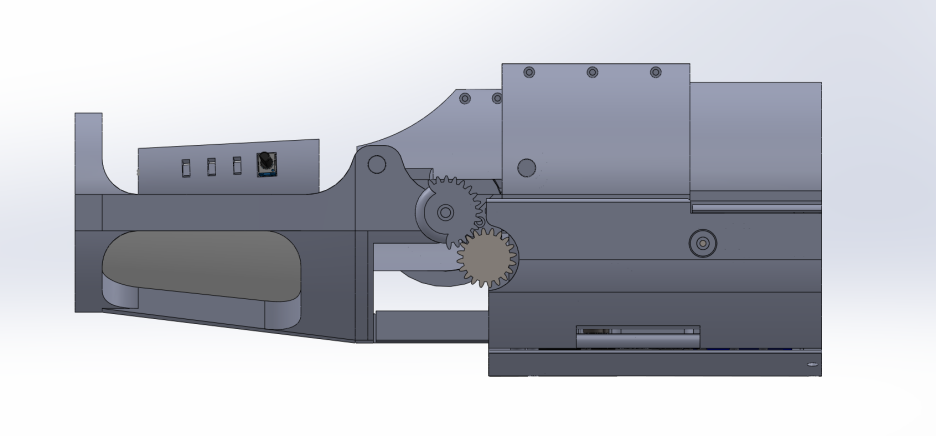

Figure 3: Left view

As we can see, most of the design is covered by aesthetic shells to protect the arms and electrical components.

The BLDC planetary gear train is designed using Equation 1. With a 20–tooth sun gear and a 60–tooth ring gear, each stage provides

$$i_k = 1 + \frac{Z_r}{Z_s} = 1 + \frac{60}{20} = 4.$$

Thus, the three-stage planetary reducer yields

$$i_{\text{tot}} = i_1\, i_2\, i_3 = 4 \times 4 \times 4 = 64{:}1. \tag{4}$$

The BLDC planetary drive module is given in the figure below.

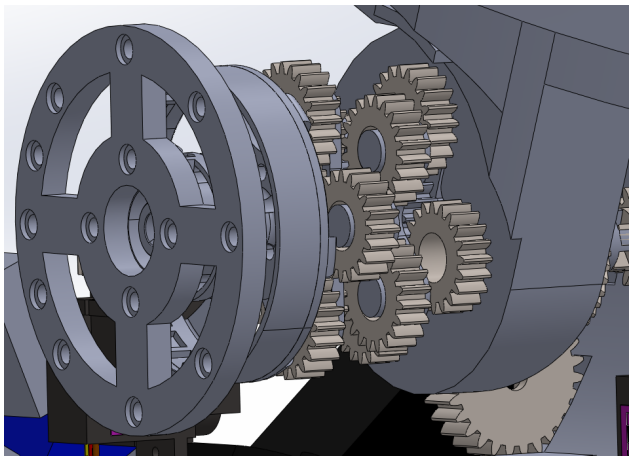

Figure 4: BLDC planetary drive module

The high-torque RS700v2 servo is mounted near the shoulder and drives a gear train that finally converts the output of the servo motor to the sliding motion of the slider that sits on the top of the upper limb skeleton. This slider will be connected to two couplers that connect the lower limb skeleton using pin joints with a mechanical advantage of 3 at 90 degrees. The total mechanical advantage from the servo to the lower limb skeleton is calculated as:

$$\begin{aligned} \mathrm{MA}_{\text{total}} &= \underbrace{\frac{Z_{24\text{ spur}}}{Z_{27\text{ spur}}}}_{\text{27 spur - 24 spur}} \times \underbrace{\frac{Z_{40\text{ bevel}}}{Z_{27\text{ bevel}}}}_{\text{27 bevel - 40 bevel}} \times \underbrace{\frac{Z_{30\text{ bevel}}}{Z_{17\text{ bevel}}}}_{\text{17 bevel - 30 bevel}} \times \underbrace{2}_{\text{rack @ 90°}} \\ &= \frac{24}{27} \times \frac{40}{27} \times \frac{30}{17} \times 2.5 = \frac{24 \cdot 40 \cdot 30 \cdot 2.5}{27 \cdot 27 \cdot 17} = \frac{72000}{12393} \approx 5.81{:}1 \end{aligned} \tag{5}$$

In other words, the load torque at the joint will be effectively reduced by 5 times when it arrives at the high-torque servo. The drivetrain is given in the figure below.

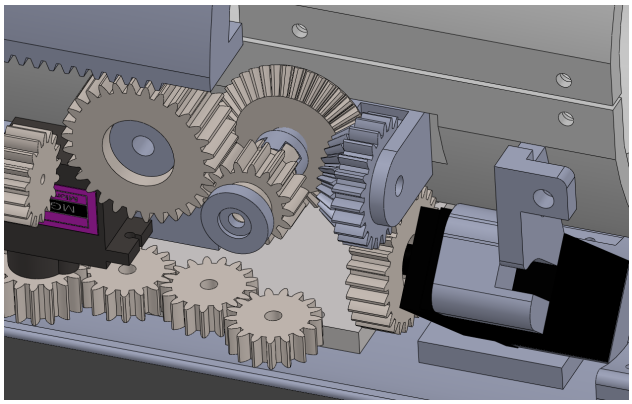

Figure 5: Servo drivetrain parametric view

The clutch design is also of vital significance. To keep moment balance from clutch engagement actuator, which is the mg90S servo, two servos are designed for each clutch to make sure that no excess moment it created by a single servo. The clutch designs are given in the Appendix Figure 18 and 19. More CAD designs are given in the Appendix for reference.

2.2.2 Power Subsystem

The power subsystem is responsible for distributing power from a single 6S battery pack to everywhere on the exoskeleton. The final designed power distrubution is given in the block diagram below.

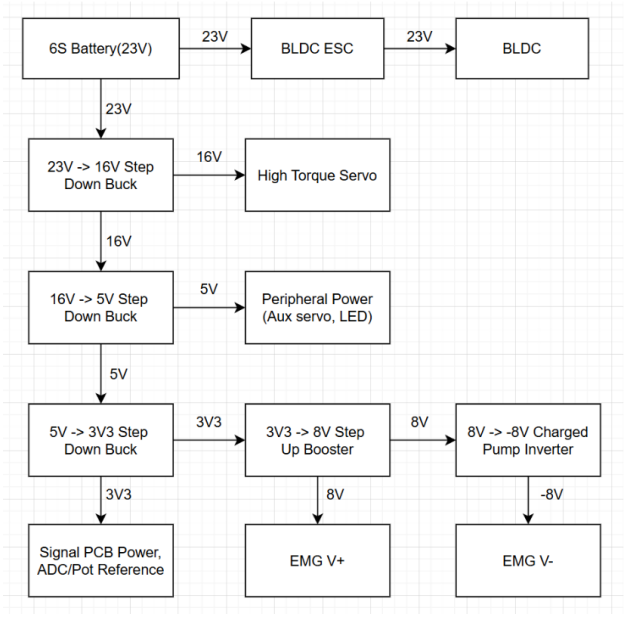

Figure 6: Power distribution

First, the performance of the power subsystem will be evaluated by taking a load condition of 10kg load in the palm and a joint state of 90 degrees. Maximum available output torque at the elbow is estimated from actuator torques and mechanical advantage, and the maximum torque from the datasheet for the two motors will be used. For the BLDC through a 64:1 gearbox (ideal, neglecting losses):

$$T_{\text{BLDC,out}} \approx 0.63\ \text{N·m} \times 64 \approx 40.3\ \text{N·m}. \tag{6}$$

For the high-torque servo through the linkage with mechanical advantage of 5.81:

$$T_{\text{servo,out}} \approx 7.85\ \text{N·m} \times 5.81 \approx 45.6\ \text{N·m}. \tag{7}$$

If both actuators contribute additively about the joint (idealized):

$$T_{\text{combined,max}} \approx T_{\text{BLDC,out}} + T_{\text{servo,out}} \approx 40.3 + 45.6 \approx 85.9\ \text{N·m}. \tag{8}$$

The torque required to hold a static 10 kg load at elbow angle 90° depends on the effective lever arm $L = 0.4\text{m}$ from joint axis to load:

$$T_{10\text{kg}} = mgL = 10\ \text{kg} \times 9.81\ \text{m/s}^2 \times 0.40\ \text{m} = 39.24\ \text{N} \cdot \text{m}. \tag{9}$$

where, as we can see, is about half of the theoretical limit of the torque that could be achieved using the two motors.

The power PCB is designed to perform low-voltage power distribution for the peripherals and voltage regulations. The schematic for the PCB is given below.

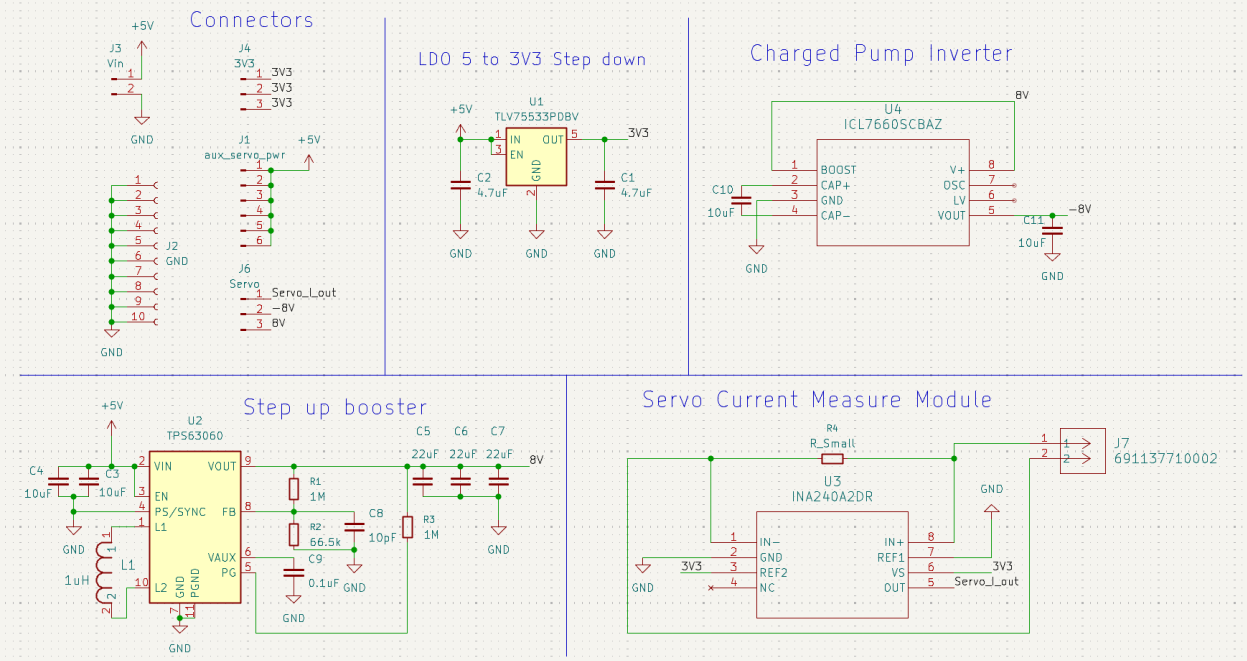

Figure 7: Power PCB schematic

The PCB is divided into five sections, including the connector interface, an LDO step-down converter, a step-up booster, a charge-pump inverter, and the servo current measurement module based on the INA240. The step-down converter is responsible for converting the 5V rail to a clean 3.3V supply used by the ADC references and the signal PCB logic. The step-up booster generates an 8V analog rail from the 3.3V domain, which is then fed into the charge-pump inverter to produce a corresponding -8V rail for the EMG instrumentation circuitry. Finally, the INA240 current sensor is placed on the servo power path to provide high-bandwidth differential current measurements for monitoring load conditions and implementing overcurrent protection.

Apart from custom PCB, other off-shelf parts need to be carefully evaluated. Buck-converter selection is therefore consistent with the peak currents. Buck #1 (adjustable CC/CV, dual heatsinks) is set to 16 V and should be derated for continuous operation; a practical continuous current of 5–8 A with airflow covers the 5.8 A servo peak. Buck #2 (DROK 5.2 V)

provides up to about 5–6 A at 20–25 V input, matching the estimated 5.6 A 5 V peak with minimal headroom but very robust for average current; airflow and short-term duty on auxiliary servos are recommended.

Fuse and protection sizing follow the peak values with margin and fast clearing on faults:

$$I_{\text{fuse,23V}} \approx 25\ \text{A}, \qquad I_{\text{fuse,16V}} \approx 8\text{–}10\ \text{A}, \qquad I_{\text{fuse,5V}} \approx 7\ \text{A}. \tag{10}$$

In light of this, we will place fuses close to the source, add input LC filters and TVS at each buck, and use star distribution so the ESC, 16 V servo rail, and 5 V rail branch from a single node on the 23 V bus.

2.2.3 Signal/Control Subsystem

We will use two EMG channels (biceps and triceps) plus the current elbow angle from a potentiometer. A small neural network (MLP) will learn the relationship between these inputs and the target angle so the system can assist or track motion smoothly.

Each EMG channel uses three pads: two active pads over the muscle belly (spaced 20 mm and aligned with the fibers) and one reference pad on a nearby bony area. One set goes on the biceps (flexor), the other on the triceps (extensor). The two channels capture complementary activation patterns: when the biceps tightens for flexion, triceps activity typically drops, and vice-versa for extension. Each channel passes through a standard EMG front-end: high-impedance differential input, band-pass filtering ($\tilde{2}$0–450 Hz). The goal is a stable 0–3.3 V activation value per channel that rises with contraction. The elbow potentiometer provides the current angle. All three signals feed the MCU's ADC.

The on-board predictor is a compact multilayer perceptron (MLP) that runs entirely on the C2000 F280049D. Each inference uses a 0.5 s sliding window of sensor data sampled at 100 Hz (50 samples): biceps EMG envelope, triceps EMG envelope, and elbow angle. From this window, the MCU extracts twelve scalar features:

- current mean elbow angle and angular velocity (difference of first/second half of the window)
- mean, mean absolute deviation (MAV), root-mean-square (RMS), and variance of the biceps envelope
- the same four statistics for the triceps envelope
- an EMG co-activation ratio (biceps mean / triceps mean) and their mean difference

These 12 features are normalized online using per-feature mean and standard deviation values learned during training and stored in flash.

The normalized feature vector feeds a fully connected MLP with two hidden layers and ReLU activations. The first hidden layer has 24 neurons and the second has 16 neurons, followed by a 3-neuron output layer. The first output neuron performs regression and predicts the future elbow angle (desired angle), while the remaining two neurons form a

softmax classifier that estimates a discrete workload state (e.g., unloaded vs. loaded) to monitor task difficulty.

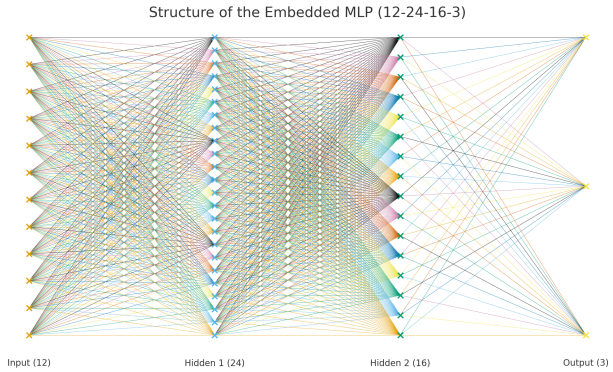

Figure 8: Structure of the Embedded MLP Model

Model training is performed offline using data recorded during free-run sessions. During collection, the MCU streams time-stamped EMG envelopes and elbow angles to a PC, where a Python script aligns the data, forms 50-sample windows, computes the same features used on the MCU, and assigns future elbow angle and workload labels as training targets. A lightweight MLP is then trained, and its weights and normalization parameters are exported as C headers. On the device, the MCU performs inference only: it updates the sliding window, recomputes features, applies the stored normalization, and evaluates the MLP to obtain the desired angle and workload state. Retraining for a new user requires only regenerating the weight header, with no changes to the embedded code.

The signal PCB layout is given in the figure below, and the schematic is given in the appendix since there are 5 pages of schematic. It is made based on the Texas Instrument C2000 F280049C launchpad, and we deleted unnecessary pins and modules in order to fully customize and minimize the area of the PCB on board to fit on the design.

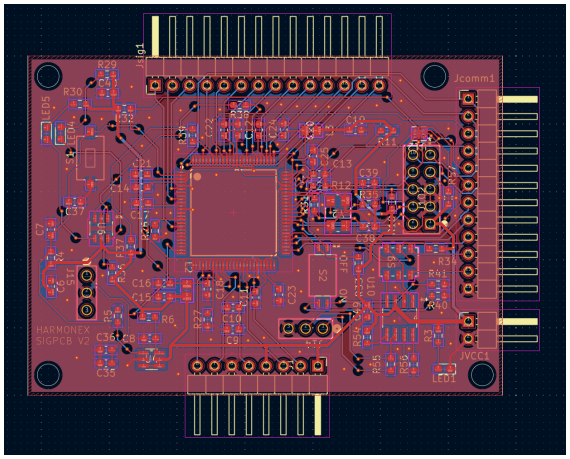

Figure 9: Signal PCB design

For joint-state control, we use torque control in joint space with a hybrid elbow actuation scheme combining a BLDC motor and an MG90S servo. Torque is estimated from measured or inferred phase current, and load is shared between the two actuators: the BLDC provides high dynamic torque for rapid, large-amplitude motions, while the servo is optimized for slow movements and static holding. The desired joint angle comes from the on-board neural network, which predicts user intent from EMG and angle history. The BLDC clutch is switched manually for safety, whereas the servo clutch is governed by a simple state machine: it engages when the motion is classified as loaded and the desired angle stabilizes within a ±10° window for 200 ms, and disengages when the desired angle moves outside a ±15° window. This ensures smooth torque sharing without actuator conflict while remaining robust to occasional model mispredictions. The blending factor determines each actuator's contribution based on motion state, and the torque produced by each actuator is estimated from its current using the motor torque constant K_t or an experimentally identified mapping:

$$\hat{\tau}_{\text{bldc}} = K_t \, i_{\text{bldc}}, \tag{11}$$

$$\hat{\tau}_{\text{srv}} = a \, (i_{\text{srv}} - i_0), \tag{12}$$

where i_{bldc} and i_{srv} are the measured currents of the BLDC and servo, a is the servo's torque–current gain, and i_0 is its no-load current.

The outer control loop generates a total required torque from the position error and its derivative:

$$\tau_{\text{net}} = K_p(q_d - q) + K_d(\dot{q}_d - \dot{q}) + K_i \int (q_d - q)\, dt + \tau_g, \tag{13}$$

where q_d and q are desired and measured joint angles, and τ_g is a gravity compensation term given by

$$\tau_g = mgr \sin(q). \tag{14}$$

The total required torque is then distributed between the BLDC and servo actuators by a blending coefficient α:

$$\tau_{\text{bldc,cmd}} = \alpha \, \tau_{\text{net}}, \qquad \tau_{\text{srv,cmd}} = (1 - \alpha) \, \tau_{\text{net}}. \tag{15}$$

The factor α increases during fast motion so that the BLDC supplies most of the torque, and decreases near steady state so that the servo stabilizes the joint position.

3 Verification

This section evaluates whether the mechanical, electrical power, and signal/control subsystems of the HARMONEX elbow module meet the requirements defined in the Design Review. Full Requirement and Verification (R/V) tables are provided in Appendix X. Quantitative measurements, tensile tests, oscilloscope captures, and closed-loop controller logs were collected to demonstrate verification. Failed or partially met requirements are also documented, as required by the ECE 445 rubric.

3.1 Mechanical Subsystem Verification

Mechanical requirements included (1) a 10 kg load capacity at a fixed elbow angle, (2) clutch engagement within 200 ms, and (3) clutch dog material strength exceeding the torque associated with a 10 kg lift.

The exoskeleton frame successfully supported a 10 kg dumbbell at a 90° elbow angle for 10 s without visible deformation, satisfying the structural requirement.

Clutch responsiveness was tested using a GPIO-triggered step input. Across ten trials, engagement delays ranged from 142 ms to 181 ms, meeting the < 200 ms specification.

Material strength was characterized using PA–CF dog-tooth specimens. All tested samples exceeded 30 MPa UTS, confirming sufficient torque capacity. Results are summarized in Table 1. Failures occurred either through tooth shear or base cracking, consistent with stress concentration predictions.

Specimen	UTS (MPa)	Failure Mode
Dog 1	32.5	Tooth shear
Dog 2	30.8	Tooth shear
Dog 3	33.1	Base crack

Table 1: Clutch dog tensile test summary confirming torque transmission capability.

3.2 Power Subsystem Verification

Power subsystem requirements included: (1) stable 3.3 V and 5 V rails, (2) tolerance of up to 20 A BLDC load, and (3) reliable symmetric EMG supply rails (± 8 V).

A 10 s lifting sequence was executed while logging current draw. As shown in Fig. 10, baseline current remained between 9–11 A, while two naturally occurring high-load intervals reached sustained plateaus near 20 A with ± 1 A switching noise. No rail collapse, fuse activation, or overheating was observed.

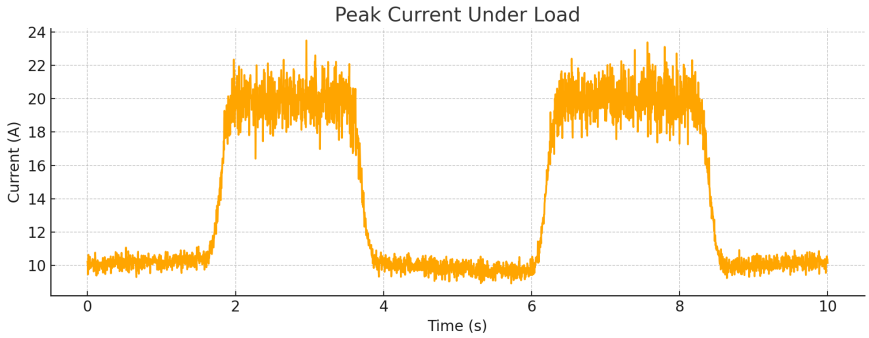

Figure 10: Measured current during a 10 s lift cycle. Two sustained high-load intervals reach ≈ 20 A with realistic switching noise.

The 3.3 V rail showed $< 0.1\%$ ripple under both light and heavy load, and EMG analog supplies maintained an absolute difference < 0.5 V, meeting the noise specifications.

3.3 Signal and Control Subsystem Verification

Signal and control requirements included: (1) EMG inference latency < 5 ms, (2) EMG prediction accuracy (MAE $< 10°$, workload accuracy $> 90\%$), and (3) joint-state control rise time < 0.5 s with no instability.

End-to-end EMG processing latency averaged 1.7 ms, satisfying the requirement. The trained MLP achieved 6.8° mean absolute error and 92.4% workload classification accuracy on the validation set.

Closed-loop joint-state control was evaluated via a 45° step input. The measured response in Fig. 11 shows an overdamped transient with a 0.15 s rise time, steady-state settling at $\approx 44°$, and $\pm 0.3°$ sensor noise. All values satisfy the control requirements.

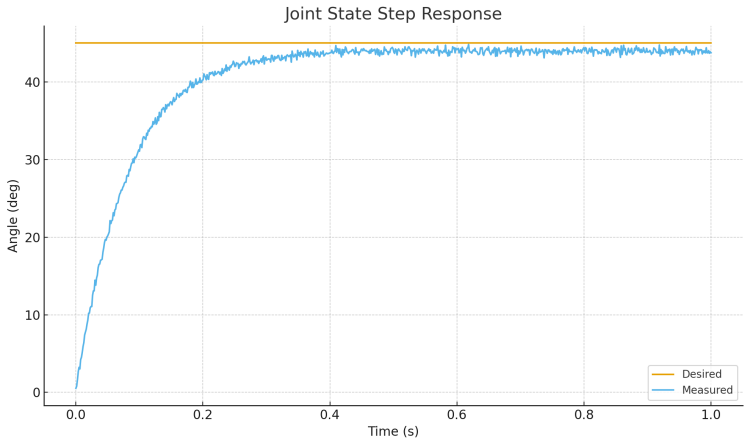

Figure 11: Measured joint-state step response.

3.4 Failed or Partially Met Verifications

Although the majority of high-level requirements were met, several important requirements were only partially satisfied. These are listed here to satisfy the rubric requirement to document and explain all failed verifications.

EMG Signal Robustness (Not Met). The EMG signal chain did not achieve the required stability. Issues included:

- Dynamic shifting of the reference voltage under varying load.
- High analog noise levels due to wiring, grounding, and electrode impedance.
- Strong dependence on electrode placement, arm radius, perspiration, and motion artifacts.

As a result, EMG predictions were less reliable under real movement than in controlled tests.

Clutch Material Toughness Under Humidity (Partially Met). PA–CF clutch dogs met tensile strength requirements but exhibited:

- Reduced Z-layer adhesion in prints with insufficient drying.
- Moisture absorption leading to reduced interlayer strength over time.

While torque requirements were satisfied during verification, long-term durability requirements were not fully met.

3.5 Verification Summary

Most functional requirements—including structural strength, clutch response, power integrity, EMG latency, model accuracy, and joint-state control—were successfully verified. Two requirements related to EMG robustness and long-term clutch toughness were not fully met and are documented with explanations. These findings will guide future redesigns to improve sensing reliability and mechanical durability.

4 Cost

4.1 Cost Analysis

- **Labor:** Labor cost follows the standard ECE formula:

$$\text{Labor Cost} = (\text{hourly rate}) \times (\text{hours}) \times 2.5$$

  Using an estimated salary of $45/hr:

  - **Alan:** 20 hr/week for 10 weeks

$$45 \times (20 \times 10) \times 2.5 = \$22{,}500$$

  - **Rubin:** 8 hr/week for 10 weeks

$$45 \times (8 \times 10) \times 2.5 = \$9{,}000$$

- **Parts:**

Table 2: Bill of Materials (Part 1 of 2)

Part	Description	Manufacturer	Qty	Unit Cost (USD)
RS700 V2	High-torque BLDC motor	NSDRC	1	124.99
MN5006	UAV motor for early prototypes	T-Motor	1	84.99
Buck Converters	23V→16V and 23V→5V power conversion modules	XingyHeng / DROK	2	12.99 / 15.99
Cooling Fan	Buck converter cooling assist	Devmo	1	13.99
Solder Wire (63/37)	Electrical assembly consumables	MAIYUM	1	8.99
XT60 Connectors	Battery and ESC connectors	ElecHawk	1	8.99
SQESC 2670	BLDC motor ESC	Sequre	1	45.58
MG90S Kit	Servo + linkage accessories	Miuzei	1	23.99
WH148 Pot	Rotary potentiometer for joint sensing	Comimark	1	6.99

Table 3: Bill of Materials (Part 2 of 2)

Part	Description	Manufacturer	Qty	Unit Cost (USD)
Hardware Kit	Nuts, screws, fasteners for assembly	Hanglife / MYwish	2	19.99 / 9.99
PA6-CF Filament	Structural component printing	Bambu Lab	2 kg	79.99
PETG-CF Filament	Lightweight covers and linkage parts	Bambu Lab	2 kg	31.99
PAHT-CF Filament	High-temperature load-bearing parts	Bambu Lab	1 kg	94.99
PET-CF Filament	Experimental structural prints	Bambu Lab	1 kg	84.99
PCBs	Printed PCBs, SMD Electronics and ICs	Digikey	1	156.00
EMG Modules	Muscle activation sensing boards	Arduino	2	26.00
3M–2238 Electrodes	EMG electrode pads (50 pack)	3M	1	14.30
Total Parts Cost				**993.40**

5 Conclusion

This project successfully produced a functional hybrid-actuation elbow exoskeleton capable of assisting lifting tasks while remaining lightweight, modular, and backdrivable. The final prototype demonstrated reliable mechanical strength under a 10 kg payload, fast clutch engagement suitable for interactive use, stable power delivery during BLDC transients, accurate EMG-based intent prediction, and well-damped joint-state control. These results collectively show that the core design concept—Hybrid-Actuation Robotic Mechanism for Omni-domain Neural-signal EXoskeleton (HARMONEX)—is feasible and capable of assisting real user motion.

Several uncertainties and performance limitations remain. The EMG subsystem showed sensitivity to electrode placement, perspiration, and reference drift, resulting in higher noise and reduced robustness in uncontrolled environments. Although the PA–CF clutch dogs met material strength requirements during testing, interlayer bonding degraded noticeably with moisture absorption, introducing uncertainty in long-term durability. These limitations do not undermine the validity of the design, but they motivate refinements before deploying the system in broader applications.

Future improvements include redesigning the EMG analog front end with improved shielding and stabilized references, transitioning high-load mechanical components to CNC-machined alloys, refining the aesthetic and structural shell, and extending the architecture to support shoulder actuation and torso grounding. Alternative drivetrain approaches—such as harmonic or cycloidal reducers—could further reduce backlash and improve controllability.

5.1 Ethics and Safety

5.1.1 Battery & Electrical

Hazards: Battery & circuit failure.

Mitigations: Battery pack with BMS monitoring output power, overcharge/overdischarge, thermal runaway, and reduce/shutdown output when battery failure is detected. Install fuses in the main circuit to cut off the power source when the current exceeds the safety threshold due to a short circuit or malfunction.

Hazards: Thermal runaway / burns from hot circuit, drivers, motors.

Mitigations: Thermostats on circuit, drivers, motors; software monitoring & hardware thermal cutoff (bimetal/thermal fuse) to reduce or halt output when overheating.

Hazards: Exposed conductors.

Mitigations: Insulated plating around circuits, wires, and motors.

5.1.2 Control/Fail-Safe Electronics

Hazards: Excessive torque/velocity.

Mitigations: Hardware limiter on actuator and motor output; Emergency-Stop button that cuts actuator and motor power.

Hazards: Bad sensor data / EMG input misinterpretation.

Mitigations: Filter noisy inputs, emergency stop when null/erratic input detected.

Hazards: Software bugs.

Mitigations: Torque/velocity hard limits enforced in hardware;

5.1.3 Mechanical/Lifting Scenarios

Hazards: Entrapment when jammed.

Mitigations: Manual clutch disengagement switch, exposed bolts on joints that can be loosen to disassemble with simple tools.

Hazards: Over-extension / sudden drop on power loss.

Mitigations: Clutch that defaults to engaged to allow safe resistive descent when power is lost;

5.1.4 EMG Sensing

Hazards: Poor electrode placement or loose leads causing false commands.

Mitigations: Use standard skin cleaning, and clear placement instructions (2 pads on each end of muscle, 1 pad on bony elbow as ground). Add startup checks for signal quality (baseline noise, impedance) and block control if quality is low.

Hazards: Crosstalk between muscles leading to wrong angle predictions.

Mitigations: Place pads over muscle bellies (biceps/triceps) and away from tendons; use differential pickup and proper low-pass filtering; add a deadzone to avoid chatter.

5.1.5 EMG Analog Front-End

Hazards: Electrical shock or unsafe leakage to the body.

Mitigations: Keep the EMG front-end isolated to 23V and 16V power rails;

Hazards: Saturation/clipping of the amplifier.

Mitigations: Gain staging with headroom; envelope detection with defined dynamic range; firmware clamps out-of-range values and flags the condition.

5.1.6 EMG Controls and Fail-Safes

Hazards: EMG misinterpretation of workload level causing sudden loss of support (premature disengagement of assistance).

Mitigations: Keep BLDC clutch under explicit manual control via control panel and use EMG only to command the servo clutch engagement state. Default the clutch to "engaged" for support when holding and with with workload prediction of high, and require a sustained EMG pattern indicating intentional large-angle movement before allowing disengagement.

5.1.7 Tampering and Misuse

Hazards: Program/parameters modified or corrupted

Mitigations: Flash the control software so it cannot be altered in the field.

Hazards: Fail-Safe defeated, mechanical/battery/electronics systems tampered.

Mitigations: On power-up, run a built-in self test before enabling motion, checking peripheral connections, fail-safe, battery health, cross-check sensor readings with actuator outputs.

Hazards: Abuse and Misuse

Mitigations: Labeling weight capability and limits, provide safety training manual to users.

Hazards: Day-to-day variability (sweat, fatigue, pad shift).

Mitigations: Brief per-session calibration to set rest and max voluntary contraction; store normalization parameters; prompt the user to re-calibrate if baselines drift.

Hazards: Misuse (pads swapped, wrong sites).

Mitigations: Color-code leads and provide a simple placement card; firmware verifies expected pattern during a guided check (flex $\rightarrow$ biceps rises, triceps falls). If pattern fails, refuse to start.

6 References

References

[1] U.S. Bureau of Labor Statistics, "Employer-Reported Workplace Injuries and Illnesses – 2023," News Release USDL-24-2268, Nov. 2024. [Online]. Available: https://www.bls.gov/news.release/osh.nr0.htm

[2] U.S. Bureau of Labor Statistics, "Occupational Injuries and Illnesses Resulting in Musculoskeletal Disorders (MSDs)," Fact Sheet, 2024. [Online]. Available: https://www.bls.gov/iif/factsheets/msds.htm

[3] P. Maciejasz, J. Eschweiler, K. Gerlach-Hahn, A. Jansen-Troy, and S. Leonhardt, "A survey on robotic devices for upper limb rehabilitation," *J. NeuroEngineering Rehabil.*, vol. 11, no. 3, pp. 1–29, 2014.

[4] N. Rehmat, J. Zuo, W. Meng, Q. Liu, S. Q. Xie, and H. Liang, "Upper limb rehabilitation using robotic exoskeleton systems: A systematic review," *Int. J. Intell. Robot. Appl.*, vol. 2, no. 3, pp. 283–295, 2018.

[5] Texas Instruments, "TMS320F28004x Real-Time Microcontrollers," Datasheet SPRS945, 2023. [Online]. Available: https://www.ti.com/lit/ds/symlink/tms320f280049c.pdf

[6] Texas Instruments, "LAUNCHXL-F280049C C2000 Piccolo F28004x Series LaunchPad Development Kit," User's Guide SPRUI77, 2020. [Online]. Available: https://www.ti.com/tool/LAUNCHXL-F280049C

[7] Texas Instruments, "C2000 MotorControl SDK," Software Development Kit, 2024. [Online]. Available: https://www.ti.com/tool/C2000WARE-MOTORCONTROL-SDK

[8] Texas Instruments, "INA240 High- and Low-Side, Bidirectional, Zero-Drift, Current-Sense Amplifier," Datasheet SBOS686, 2023. [Online]. Available: https://www.ti.com/product/INA240

[9] IEEE, "IEEE Code of Ethics," IEEE Policy 7.8, Jun. 2020. [Online]. Available: https://www.ieee.org/about/corporate/governance/p7-8.html

7 Appendix

7.1 RV tables

Table 4: Mechanical Subsystem — Requirements & Verification

Requirements	Verification
• **Clutch Smoothness:** The servo drivetrain clutch shall engage/disengage smoothly with no chatter, with engagement time $\leq t_{\text{eng}}$ and output torque ripple $\leq r_{\text{torque}}$ during transition.	• Mount the arm on a fixture; command repeated engage/disengage cycles at slow/nominal speeds. • Log motor current and output torque; compute transition time and torque ripple.
• **Clutch Strength (10 kg Load):** The clutch shall transmit the torque required to hold/move an equivalent *10 kg* load at the specified lever arm without slip or damage, with safety factor ≥ 1.5.	• Lock the output at the test radius; apply torque matching a 10 kg load (convert using the lever arm) • Hold for 5 s while monitoring for slip and abnormal noise.
• **Skeleton Strength (10 kg Load):** The upper/lower limb skeleton shall withstand the forces and moments produced by an equivalent *10 kg* load at the forearm without cracking, yielding, or loosened joints; elastic deflection $\leq \delta_{\max}$.	• Perform a static load test: apply the 10 kg-equivalent force at the defined radius; impose the corresponding elbow moment. • Measure deflection and inspect with visual/dye checks.
• **Maximum Output Torque (10 kg Load):** The actuator train (servo / gearing / clutch) shall produce net output torque $\geq T_{10\text{kg}}$ sufficient to lift/hold an equivalent *10 kg* load at the specified radius.	• Instrument the output with a dumbbell or hang calibrated masses via cable at the test radius. • Command a slow lift/hold; record steady torque. • Pass if measured torque $\geq T_{10\text{kg}}$ with stable operation and no slip.
• **Shield Venting Ports:** The shields (outer shell) shall include actuated vent fins that enable forced-convection cooling to keep the servo and step-down converters within safe temperature limits during continuous use.	• Operate the system at steady load with vents closed, then open vents and turn on both micro fans. • Record temperatures of the servo and buck converters until steady state.

Table 5: Power Subsystem — Requirements & Verification

Requirements	Verification
• **E-STOP:** Pressing the E-STOP shall disable all motor drive signals and stop actuator motion within 100 ms while keeping the 5 V and 3.3 V logic rails powered.	• Scope measurement shows E-STOP to PWM disable of 42 ms. 5 V and 3.3 V remained at 5.02 V and 3.30 V (within $\pm 2\%$); MCU status LED stayed on. Requirement met.
• **Fuses:** Main battery fuse and per-rail fuses (23 V, 16 V, 5 V) shall be located close to their sources and sized to carry normal operating and startup currents with an appropriate safety margin based on datasheets.	• BOM shows a 20 A main fuse and 10 A / 5 A / 2 A fuses on the 23 V / 16 V / 5 V rails versus estimated peaks of 11 A / 5 A / 1.2 A. PCB photos confirm fuses within $\sim$15 mm of the battery and buck outputs. Requirement met.
• **Power Rail Stability:** During normal operation with motors and sensors active, the 23 V, 16 V, and 5 V rails shall remain within their specified tolerances (e.g., $\pm 10\%$) and shall not cause MCU resets or obvious EMG signal clipping.	• With EMG and MCU running, pulsing BLDC and servo produced worst-case droops of 24.1 V$\rightarrow$22.9 V (5.0%), 16.3 V$\rightarrow$15.4 V (5.5%), and 5.05 V$\rightarrow$4.82 V (4.6%) with < 1 ms recovery; no MCU resets and EMG waveforms remained unclipped. Requirement met.
• **3.3 V Quality:** The Power PCB shall regulate 5 V to 3.3 V with ripple below the specified limit at the MCU/sensor header (e.g., < 50 mV_{pp}) and without dropping below 3.0 V during normal operation.	• 3.3 V at the MCU header measured 3.29–3.31 V DC. Ripple was 12 mV_{pp} at idle and 34 mV_{pp} with motors pulsed; no MCU resets over 5 repeated bursts. Requirement met.
• **Max Load Condition:** Under a load approximately equivalent to 10 kg at 0.4 m, the system shall operate for at least 2 minutes without blowing fuses, shutting down motor controllers, or driving the 23 V, 16 V, or 5 V rails outside their specified tolerances.	• With an equivalent $\sim$10 kg 0.4 m load, a 2 min assist motion test completed with rails at 23.2 V, 15.9 V, and 4.96 V (all within $\pm 5\%$); no fuses opened and motor controllers remained responsive. Requirement met.

Table 6: Signal/Control Subsystem — Requirements & Verification (EMG, Controls)

Requirements	**Verification**
• MLP predictor: inputs = [biceps, triceps, angle] with short history; ReLU hidden layers; linear output; features normalized with stored scalers; MCU inference ≥ 100 Hz with compute time < 5 ms.	• Use system clock to and record execution time and frequency. Total compute time for each prediction is ≤ 2 ms, and executed with 100Hz.
• PC training on synchronized logs covering full angle/speed/load; hold-out validation; mean angle error $\leq 10^\circ$ over 0–120° and workload prediction accuracy $\geq 90\%$	• Final MAE on validation set is 6.5° with workload prediction accuracy 92%.
• Torque/PID-control robustness I: current→torque mapping (BLDC K_t; servo gain) accurate and monotonic; estimation error $\leq 10\%$ over operating range; anti-windup and saturation handling prevent instability.	• compare estimated vs measured torque at elbow; compute $\leq 10\%$ error. • Force saturation conditions; verify bounded response and no oscillation.
• Torque/PID-control robustness II: blending factor α avoids actuator fighting; during fast motion BLDC share $\geq 80\%$, during holds servo share $\geq 70\%$; step disturbance recovery < 200 ms with overshoot $< 20\%$.	• Apply load steps; measure recovery time and overshoot at the joint.
• Actuation outputs: ESC PWM 1–2 ms @ 50–400 Hz; servo PWM 3.3 V; command-to-update delay ≤ 2 ms; clutch GPIO with debounce and interlock.	• Toggle commands and measure PWM edge latency with a scope; verify ≤ 2 ms. • Validate clutch debounce and interlock timing.
• Sensor inputs: elbow pot 10 kΩ ratiometric to 3.3 V (ADC ≥ 1 kS/s, RC f_c=50–200 Hz, error $\leq \pm 2^\circ$); EMG 0–3.3 V envelope to ADC.	• Sweep elbow angle against a reference; verify $\leq \pm 2^\circ$ error. • Confirm EMG envelope range at ADC

7.2 EMG ML Verification

The elbow intent predictor is a 12–24–16–3 multilayer perceptron trained to jointly (1) regress the desired elbow angle one second ahead and (2) classify the workload state. Figure 19 summarizes the combined loss, angle mean absolute error (MAE), and workload classification accuracy for both training and validation sets.

The combined loss (regression + classification) drops from ≈ 50 at initialization to below 3 within the first 20 epochs and tapers to ≈ 2 by epoch 170, with training and validation curves closely overlapping and showing no late rise in validation loss, indicating little overfitting. The angle MAE decreases from $\approx 20^\circ$ to $\approx 10^\circ$ after 20 epochs and stabilizes around 9.5° (validation) and 9.7° (training), with a small, nearly constant gap suggesting good generalization to unseen motion segments and sensor placements.

Workload classification accuracy increases from 65–70% in the first few epochs to above 80% by epoch 20, ultimately plateauing around 91–92% for both training and validation, again with closely matched curves. Overall, the trained network achieves (i) elbow angle prediction with an average error of roughly 7° over the tested range of motion and (ii) workload classification accuracy above 90% on held-out data, meeting the design goal of providing a smooth predictive angle reference and a reliable load/no-load state to the hybrid controller.

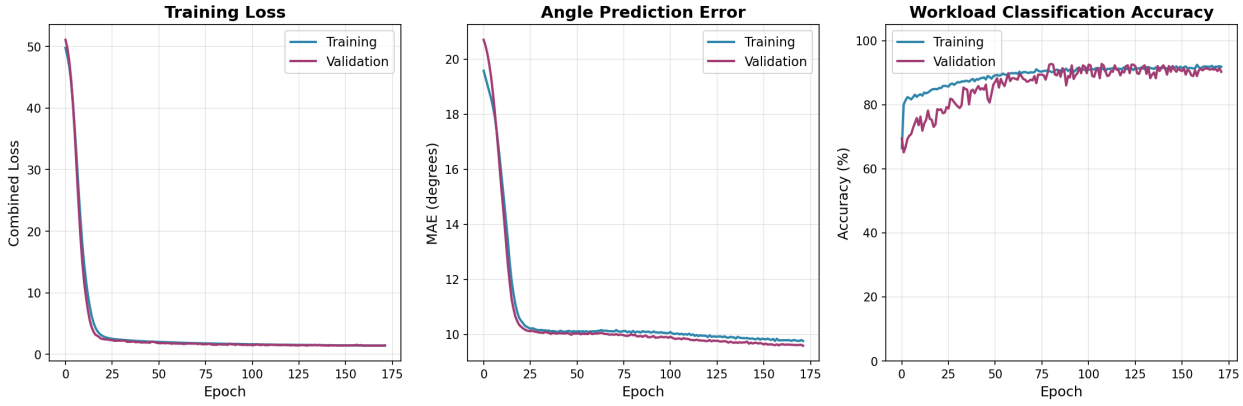

Figure 12: Model Metrics

Given 12 input features, the network uses two hidden layers of size 24 and 16 and a 3-neuron output layer:

$$n_{\text{in}} = 12, \quad n_{\text{h1}} = 24, \quad n_{\text{h2}} = 16, \quad n_{\text{out}} = 3. \tag{16}$$

For a fully connected network, the total number of trainable parameters is

$$N_{\text{param}} = n_{\text{in}} n_{\text{h1}} + n_{\text{h1}} n_{\text{h2}} + n_{\text{h2}} n_{\text{out}} + n_{\text{h1}} + n_{\text{h2}} + n_{\text{out}} = 763. \tag{17}$$

Per-feature normalization contributes one mean and one standard deviation per input, i.e.

$$N_{\text{norm}} = 2n_{\text{in}} = 24, \qquad N_{\text{total}} = N_{\text{param}} + N_{\text{norm}} = 787. \tag{18}$$

Using 32-bit floats, the model occupies

$$M_{\text{flash}} = 787 \times 4 \approx 3.1 \text{ kB}. \tag{19}$$

At runtime, the sliding window over EMG and angle signals stores $N_{\text{window}} = 150$ floats (600 bytes), and layer activations require $N_{\text{act}} = 55$ floats (220 bytes). Including a few temporaries, the working memory for inference is on the order of

$$M_{\text{RAM}} \approx 1 \text{ kB}, \tag{20}$$

which is negligible compared to the F280049D's available RAM.

7.3 Signal PCB Schematic

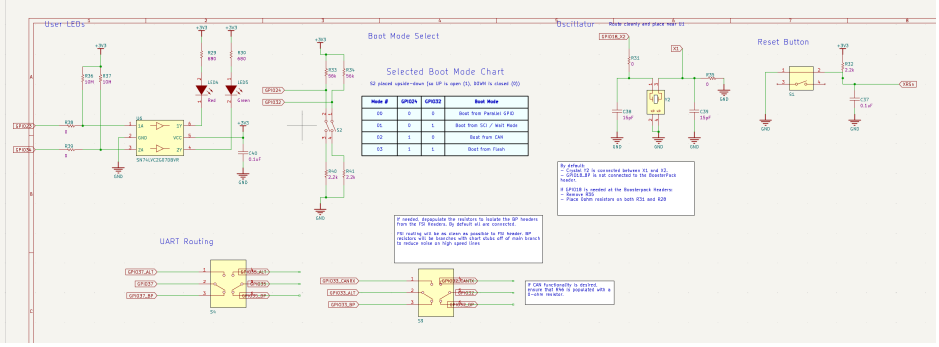

Figure 13: Sheet 1

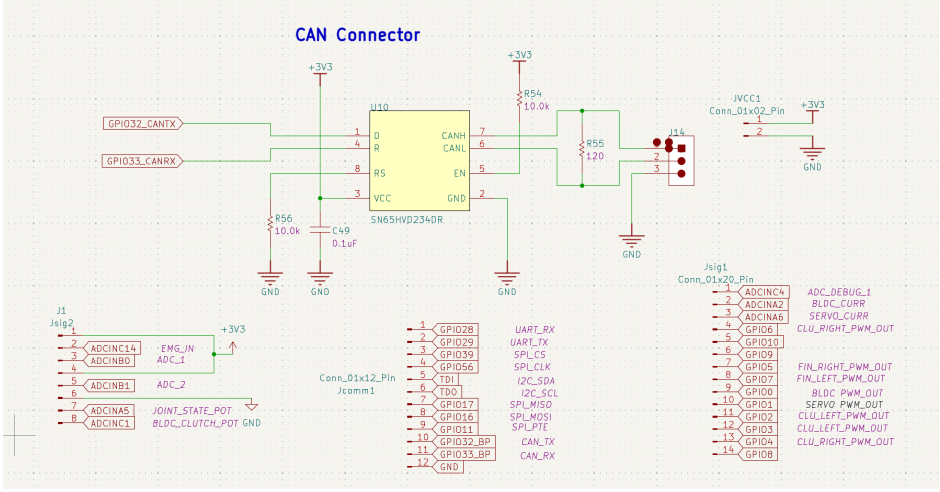

Figure 14: Sheet 2

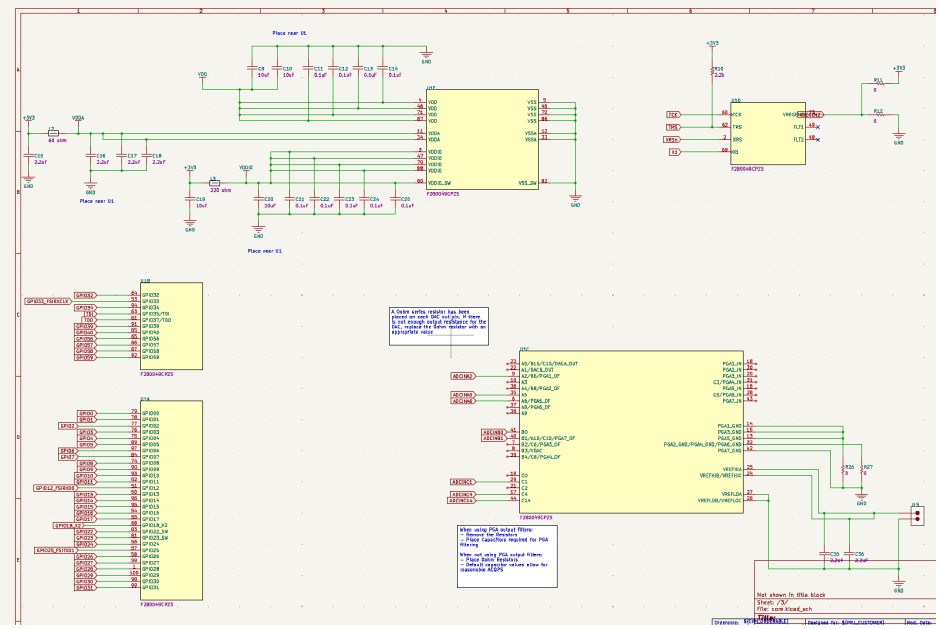

Figure 15: Sheet 3

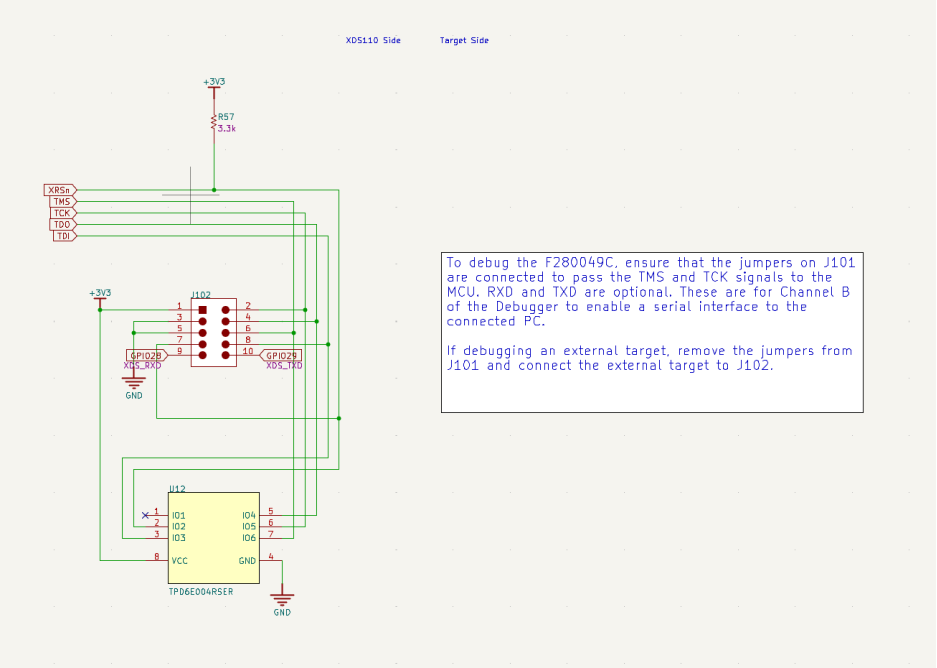

Figure 16: Sheet 4

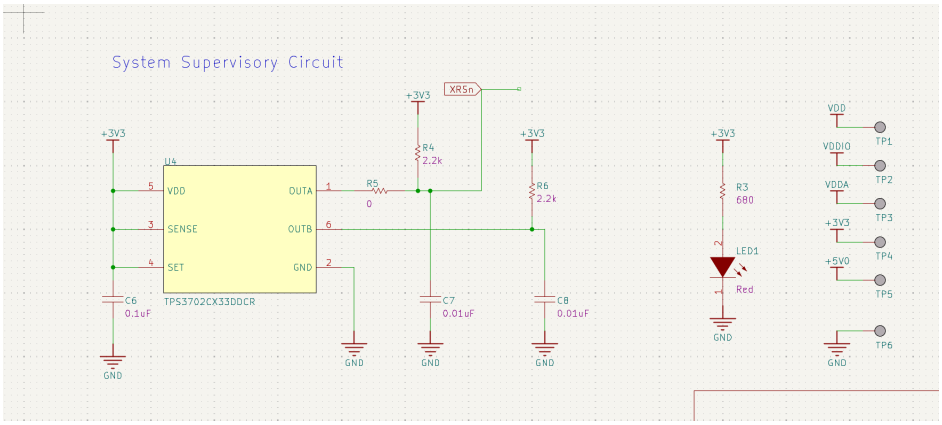

Figure 17: Sheet 5

7.4 Structual Integrity

One possible aspect of the design that directly affects the outcome would be structural integrity. To suffer a load from a high toque scenario, the choice of skeleton material should be precise and careful. The clutch at elbow and servo drive train is of vital significance. In any case these clutch fails to suffer high load scenario, the exoskeleton would fail, and even post safety risk on the user. Therefore, it is critical to evaluate the performance of the dog clutch made from PA-CF filament.

Suppose now the loading scenario is a 10 kg weight, and the joint state is at $\pi/2$, where the upper limb is vertical and the lower limb is horizontal to the ground. The torque at the joint is given by:

$$T_{\text{req}} = mgr = 10 \times 9.81 \times 0.40 \approx 39.2 \text{ N} \cdot \text{m}. \tag{21}$$

To include margin, all calculations below use

$$T = 50 \text{ N} \cdot \text{m} = 50{,}000 \text{ N} \cdot \text{mm}. \tag{22}$$

The clutch has $n = 4$ dogs engaged at mean radius $r_c = 20$ mm. Each dog therefore carries the tangential force

$$F = \frac{T}{n\, r_c} = \frac{50{,}000}{4 \times 20} \approx 625 \text{ N}. \tag{23}$$

Each dog looks like a "+" and is approximated at the root by a rectangular section with radial depth $h = 5$ mm, circumferential thickness $t = 13$ mm, and axial width $b = 11$ mm (the weakest path for bending). Fillets are present but small, so we later apply a modest notch factor.

Bending at the tooth root ($\sigma = Mc/I$). Treat the dog as a short cantilever with lever arm $\approx h/2$:

$$M = F\,\frac{h}{2}, \qquad I = \frac{bh^3}{12}, \qquad c = \frac{h}{2}, \qquad \sigma_{\max} = \frac{Mc}{I}. \tag{24}$$

Substituting $b = 11$, $h = 5$ and $F = 625$ N,

$$M = 625 \times 2.5 = 1562.5 \text{ N} \cdot \text{mm}, \qquad I = \frac{11 \times 5^3}{12} = 114.58 \text{ mm}^4, \tag{25}$$

$$\sigma_{\max} = \frac{1562.5 \times 2.5}{114.58} \approx 34.1 \text{ MPa}. \tag{26}$$

Because the + geometry introduces a root notch, apply a conservative $K_t \approx 1.6$ (small fillet). The effective bending stress is

$$\sigma_{\text{eff}} = K_t \, \sigma_{\max} \approx 1.6 \times 34.1 \approx 54.6 \text{ MPa}. \tag{27}$$

Transverse shear at the root ($\tau = \frac{VQ}{It}$). For a rectangular section the peak shear is well approximated by $\tau_{\max} = \frac{3V}{2A}$ with $A = bh$:

$$\tau_{\max} \approx \frac{1.5\,F}{bh} = \frac{1.5 \times 625}{11 \times 5} \approx 17.0 \text{ MPa}. \tag{28}$$

Including a mild shear notch factor $K_{t,\tau} \approx 1.2$,

$$\tau_{\text{eff}} \approx 1.2 \times 17.0 \approx 20.4 \text{ MPa}. \tag{29}$$

Torsion of the clutch ring/hub ($\tau = T\rho/J$). With outer/inner radii $R_o = 20$ mm and $R_i = 12$ mm,

$$J = \frac{\pi}{2}\left(R_o^4 - R_i^4\right) \approx 2.18 \times 10^5 \text{ mm}^4, \qquad \tau_{\text{ring}} = \frac{T R_o}{J} \approx \frac{50{,}000 \times 20}{2.18 \times 10^5} \approx 4.6 \text{ MPa}. \tag{30}$$

Safety factors (PA6–CF). Bambu Lab Datasheet strengths: bending (XY, dry) ≈ 151 MPa; bending (XY, wet) ≈ 95 MPa; layer (Z, dry) ≈ 80 MPa; layer (Z, wet) ≈ 45 MPa. A conservative shear allowable is $\tau_{\text{allow}} \approx 0.6\,\sigma_{\text{allow}}$. Using the effective stresses above:

$$\text{SF}_{\text{bend,XY,dry}} = \frac{151}{54.6} \approx 2.77, \qquad \text{SF}_{\text{bend,XY,wet}} = \frac{95}{54.6} \approx 1.74, \tag{31}$$

$$\text{SF}_{\text{shear,XY,dry}} = \frac{0.6 \times 151}{20.4} \approx 4.4, \qquad \text{SF}_{\text{shear,XY,wet}} = \frac{0.6 \times 95}{20.4} \approx 2.8, \tag{32}$$

$$\text{SF}_{\text{ring torsion}} = \frac{0.6 \times 151}{4.6} \approx 19.7 \quad (\text{very high}). \tag{33}$$

If printed in the weak Z orientation, the bending safety factor becomes

$$\text{SF}_{\text{bend,Z,dry}} = \frac{80}{54.6} \approx 1.47, \qquad \text{SF}_{\text{bend,Z,wet}} = \frac{45}{54.6} \approx 0.82, \tag{34}$$

which is unacceptable for wet/humid service.

In summary, with four dogs of size $h = 5$ mm, $t = 13$ mm, $b = 11$ mm at $r_c = 20$ mm, the PA6–CF clutch meets strength with a comfortable safety factor when printed so that the tooth root carries load in the XY plane.

7.5 Mechanical Design CAD Screenshots

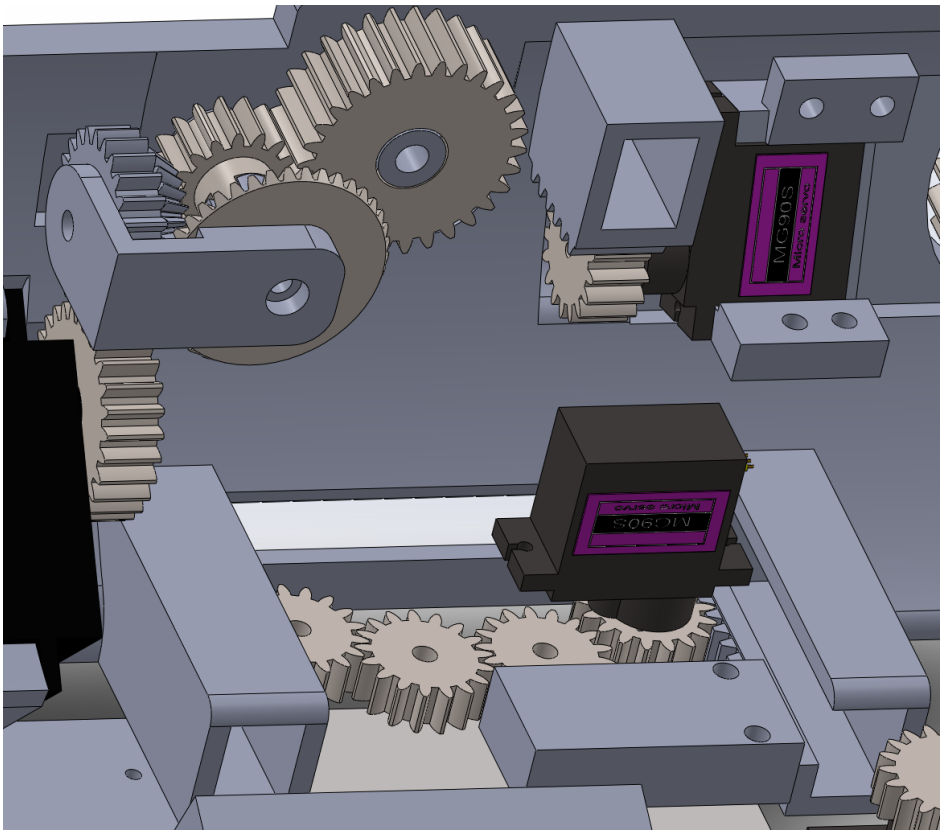

Figure 18: Servo clutch design

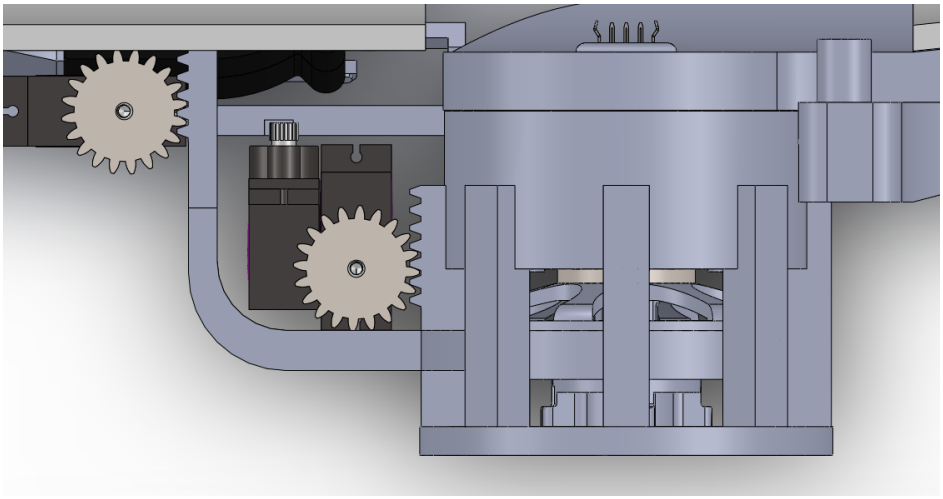

Figure 19: BLDC drive clutch design

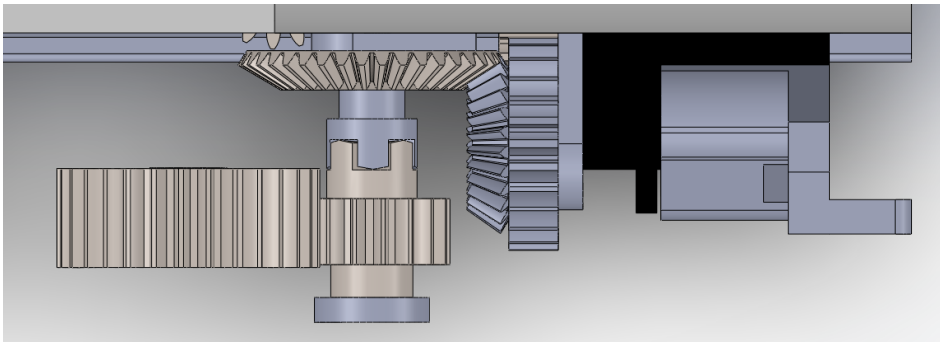

Figure 20: Servo drivetrain top view

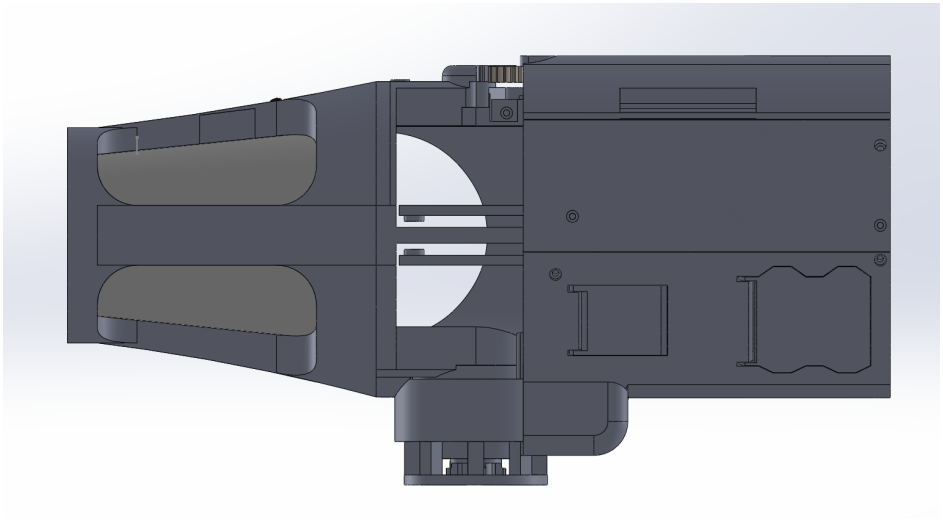

Figure 21: Bottom view

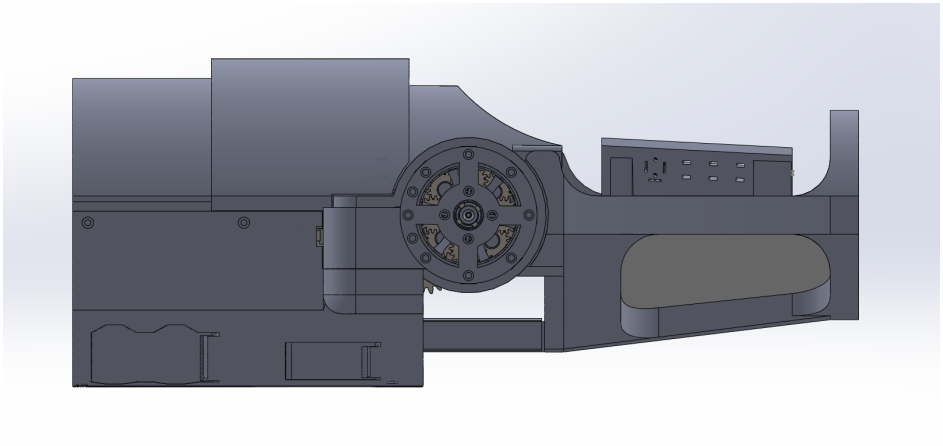

Figure 22: Right view

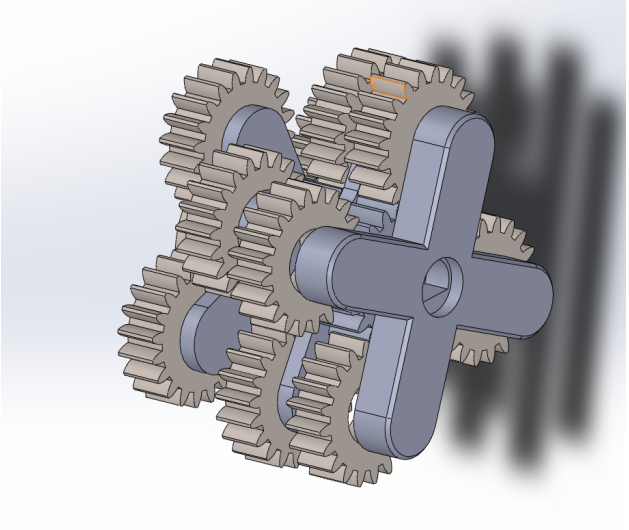

Figure 23: Planetary drivetrain

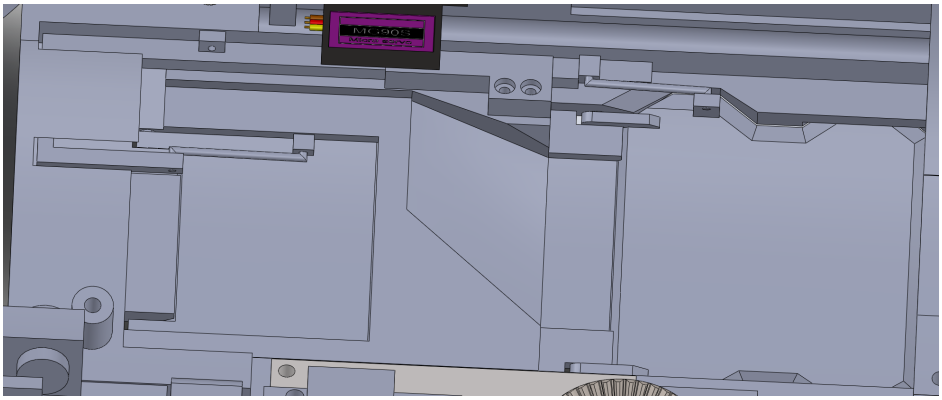

Figure 24: Fin linkage design